# Erosion-corrosion maps for carbon steel in crude oil/water slurries: impact angle and applied potential effects

**G. H. Abdulrahman and M.M. Stack**

**Department of Mechanical Engineering**

**Strathclyde University**

**75 Montrose Street**

**G1 1XJ**

**Glasgow.UK**

**Email:**

Ghaith.abdulrahman@strath.ac.uk
**m.m.stack@mecheng.strath.ac.uk**

**Phone No: +44 141 5483754**
**Fax No: +44 141 552 5105**

## Abstract

In studies of erosion-corrosion, there have been few investigations into the effect of tribological issues, such as particle impact and impact angle, on erosion-corrosion of materials in oil field production. Despite this fact, erosion-corrosion in such environments is a major issue. In such conditions, it is important to define regimes where the effect of lubricating oil may modify the erosion properties of the materials.

In this study, the combined effects of erosion and corrosion were investigated in three environments, crude oil (high API gravity 52), reservoir water, and 20% reservoir water with crude oil at a range of applied potentials. Erosion-corrosion maps were constructed, based on the results, showing the change in mechanisms and wastage rates as a function of impact angle and applied potential. Regimes of erosion-corrosion were described on such maps using such an approach.

From this work, it can be seen that the corrosion contribution was increased with an increase in the percentage of reservoir water. In the crude oil environment, it was shown that the erosion contribution (Ke) was generally higher than that for corrosion suggesting that corrosion was reduced in crude oil. The results are interpreted in terms of the effect of the crude oil environment in modifying the impact properties of the

particles therefore providing surprising resistance to particle impacts in nominally aggressive corrosion environments.

## 1. Introduction

Erosion-corrosion is a serious issue in petroleum production due to the material degradation identified in valves, pipelines and pumps in downstream and upstream conditions (1, 2). The extent of wastage depends on various parameters related to the properties of particles, the environment and the materials of the pipeline. Today, significant resources are involved in addressing erosion-corrosion issues in oil fields due to the effect of erosion-corrosion (3) and various researches have been carried out to address these issues (3-8).

Sand production from reservoir conditions can be controlled by design of a gravel pack which prevents sand from combining with oil in the process from moving from downstream to upstream conditions (3). In such conditions, corrosion occurs due to $H_2S$ (sour corrosion) and $CO_2$ (sweet corrosion) (3). Predicting the service life of the material mechanism in oil production activities under these conditions is approached with some difficulty and hence major losses in production rates have been reported due to materials issues involving erosion-corrosion in such environments(3).

In this paper, the effects of impact angle and applied potential were assessed for carbon steel in a range of crude oil/water slurries. Erosion-corrosion maps were generated based on the results showing the variation in wastage and regime of degradation as a function of these variables. The potential applications of the maps to such materials issues in petroleum production are described in this paper.

## 2. Experimental details:

### *2.1 Materials and test procedure*

Erosion–corrosion tests were performed on carbon steel X52. The dimensions of the specimens were 25mm×10mm× 4mm. In order to avoid corrosion of the area surrounding the wear scar, this area was masked off using a coating. The surface region of the sample exposed to the slurry jet was $0.19cm^2$. The samples were weighed before and after the test in order to measure mass loss and determine the erosion slurry of the samples using a Metter electronic balance.

The impact angles for the exposure tests were fixed at 15°, 30°, 45°, 60°, 75 and 90° to the impinging jet at $2.5m\,s^{-1}$.Erosion–corrosion tests were conducted for 30 minutes. Following exposure, the microstructure of the surface and mechanisms of erosion were assessed using Scanning Electron Microscopy (SEM).

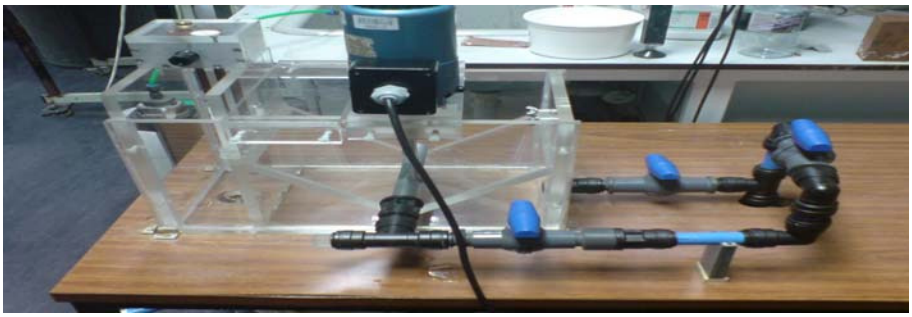

Figure (**1**) Erosion-corrosion test rig


Figure (**2**) Electrochemical interface with three electrodes ACM (Gillac).

In this work, the erosion–corrosion performance was investigated using an impinging jet apparatus, Fig. 1 (8). The slurry consisted of silica sand with a size in the range of 600-710 $\mu m$ . The pH of the solution was 8.2. Polarization curves were measured at the required impact angles and applied potentials by sweeping the potential in the anodic direction from −800 to 800 mV at a sweep rate of 200mV $min^{-1}$. Erosion–corrosion tests in potentiostatic conditions were carried out at three applied potentials of -400 mV, 0 mV and 400 mV for 30 minutes using a computer controlled ACM potentiostatic (GILLAC), Fig. 2. It should be noted that due to solution resistance, there was a drop in the applied potential of the carbon steel in crude oil environment.

## 3. Results

### 3.1 Electrochemical monitoring

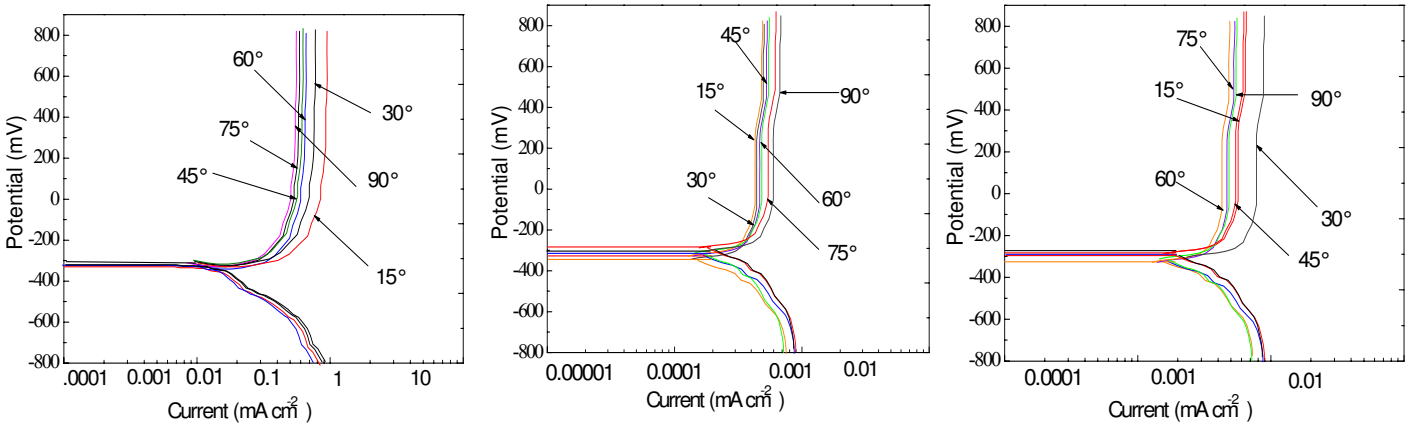


(a) (b) (c )

Figure (3) Polarization curves for carbon steel in (a) water, (b) crude oil and (c) crude oil/ 20% water at impact velocity 2.5 m $s^{-1}$.

The polarization curves, Fig. 3, indicate an active to passive transition in the conditions, with the current density being highest in water, Fig. 3(a), and lowest in oil, Fig.3(c). It was interesting that for the effect of impact angle, the maximum current density was recorded at 30$^{o}$ in the water and water/oil conditions, Figs. 3(a, c)). In the crude oil conditions, the maximum corrosion current density was recorded at 90$^{o}$.

The results indicated that the cathodic current densities were higher than those of the anodic values in the oil, Fig. 3(d), suggesting an enhancement of the cathodic reaction in the oil. This is addressed further below.

### 3.2. Volume loss and microscopy results

For the volume loss results, Kec represented the measured erosion-corrosion rate. Kc was calculated from the Faradic conversion of the current density to mass loss. The Ke, the erosion contribution, was calculated from the equation:

$$Kec = Ke + Kc \qquad (1)$$

The volume loss results, Fig. 4, in water indicate no clear pattern of erosion-corrosion rate with increasing impact angle at -400 and 0mV, Fig. 4(a-b). However, at higher potentials, i.e. at 400 mV, there was a maximum in the erosion-corrosion rate with impact angle at 45$^{o}$. By contrast, the corrosion rate tended to increase with impact angle at 400 mV in the water environment.

In the crude oil environment, Fig. 5, the value of Kc was significantly lower than Ke and Kc. The erosion-corrosion rate appeared to be independent of impact angle. By contrast in the oil/water conditions, Fig. 6, the total erosion-corrosion rate appeared to be a maximum at intermediate impact angles, with the peak impact angle of 45$^{o}$ shifting to 30$^{o}$ as the applied potential increased from 0 to 400 mV, Fig. 6(c-d).
The values of Kc in the oil water conditions, Fig. 6, were lower than those in water, Fig. 4, and higher than those than in oil, Fig. 5.This was consistent with trends shown in the polarization curves, Fig. 3.

The microscopy results, Fig. 7, indicated evidence of deformation of the surface in water, Fig. 7(a). A very smooth surface by contrast was identified in crude oil, Fig. 7(b), whereas the morphology in the mixed environment was relatively featureless in some areas, whilst showing significant evidence of erosion in other locations.

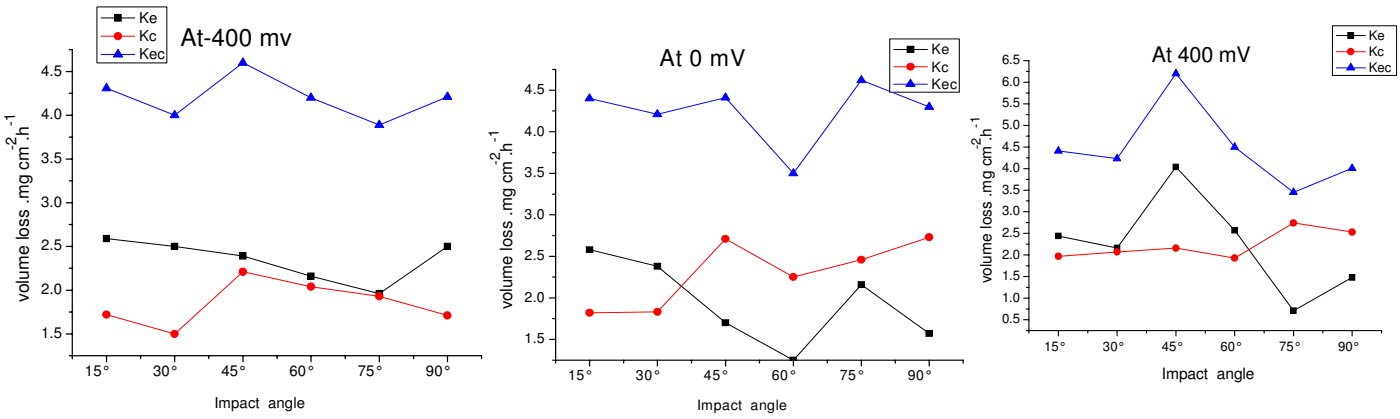


Figure (4).Volume loss as function of impact angle for carbon steel in water at 2.5 m s$^{-1}$.

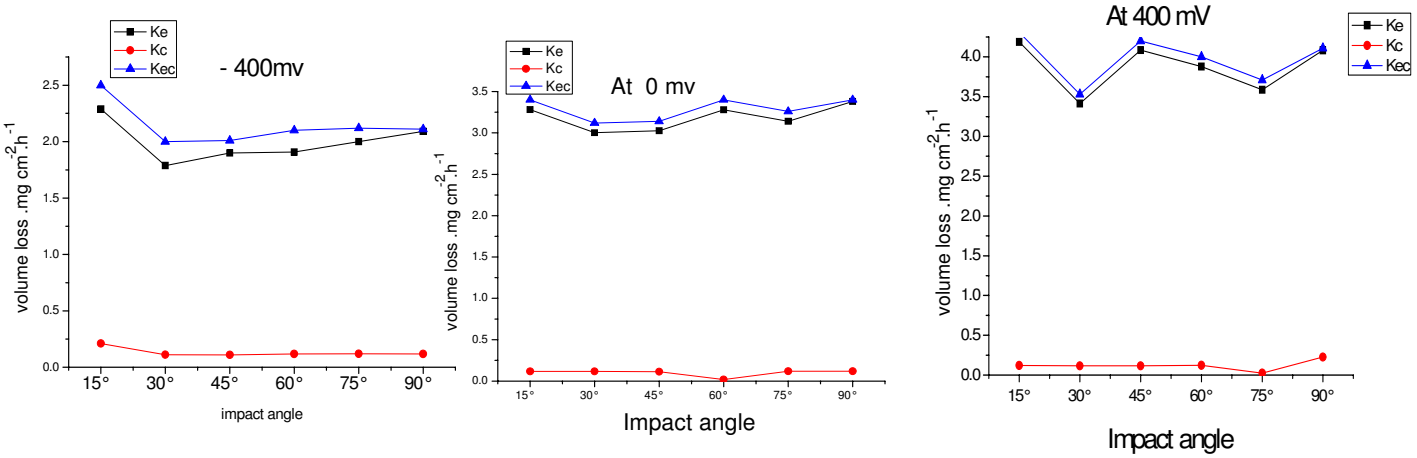


Figure (5) Volume loss as function of impact angles for carbon steel in crude oil at 2.5 m $s^{-1}$ .

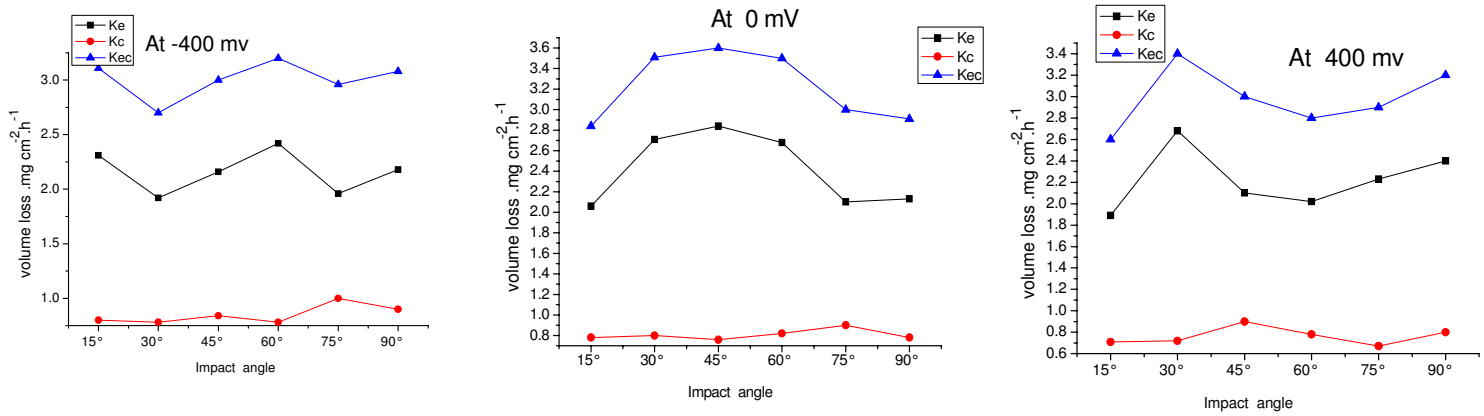


Figure (6) volume losses as function of impact angles for carbon steel in crude oil/ 20% of water at 2.5 m $s^{-1}$.

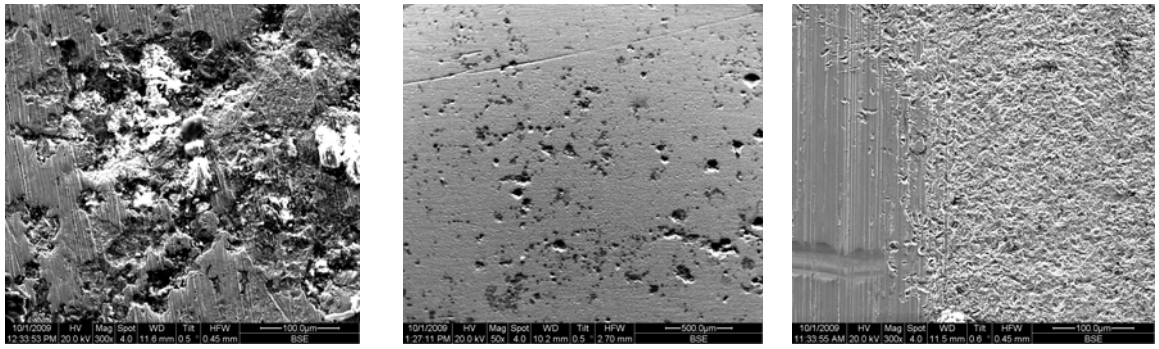

(a) (b) (c )

Figure (7): Scanning electron micrographs of eroded carbon steel test specimen at 2.5 m $s^{-1}$ , -400mV and impact angle 15°:(a) water (b) crude oil (c) crude oil/ 20% water.

## 4. Discussion

### 4.1 Trends on the effect of weight change as a function of impact angle and applied potential

The results indicate that there is a significant reduction in the corrosion current density, Fig. 3, when the experimental conditions are changed from water to crude oil. The results for the crude oil/water slurry indicate current densities intermediate between those recorded in the two environments. This indicates that corrosion is reduced significantly in crude oil environments and this is attributed to the reduction in diffusion of iron ions in the oil environments. On the other hand, the diffusion of oxygen is higher in oil than in water and this is the possibly the reason why the cathodic current densities are higher than the anodic current densities in the oil environment, Fig. 3(a) as indicated in other work (9).

The effect of impact angle shows surprising trends both on the polarization behaviour Fig. 3, and the mass loss data, Figs. 4-6. In the water environments where film formation is favoured, once the surface passivates, a maximum in the corrosion current is observed at $30^{o}$, Fig. 3(a, c), unlike that which is observed in the oil environment, where the maximum recorded is at $90^{o}$. This indicates that in environments where formation of a corrosion product is favoured, impingement at shallow impacts tends to cause higher degradation rates. The reasons why the trends differ in the oil environment are unclear at present but may be due to the physics of particle impingement in the more highly lubricated surface.

The effect of impact angle at various applied potentials shows no clear trends in the water conditions, Fig. 4. In the oil environment, Fig. 5, there is a marginally higher mass loss at 400 mV, Fig. 5 (c) compared to that observed at lower potentials. The trends for the effect of impact angle indicate that the maximum is at $90^{o}$, consistent with results on the polarization data, Fig. 3 and indicative that the cutting ability of the particle impacts may reduce in such environments. In the oil water environments, there is a clear indication of a maximum erosion-corrosion rate at intermediate impact angles, Fig. 6(b), with this maximum reducing to lower impact angles at more anodic potentials, Fig. 6(c). Clearly the reduction in lubricity reduces the erosion resistance of the layer, whilst increasing the film formed in the surface, available for removal.

### 4.2 Erosion-corrosion maps

Erosion-corrosion (Kec) maps were constructed to show that the transition between wastage regimes i.e. with the low value defined as less or equal to 6 mg $cm^{-2}$ $h^{-1}$. h, medium between 6 and 50 mg $cm^{-2}$ $h^{-1}$ and high greater or equal to 50 mg $cm^{-2}$ $h^{-1}$ (2, 4-5).
The maps, Fig. 8, indicate low wastage for all these environments under these criteria. By contrast, the erosion-corrosion mechanism maps show distinct changes in the regimes as a function of impact angle and potential. Tables 1-3 show the various Ke, Kc and Kec values.

The transitions are defined as follows:

| | | |
|---|---|---|
| Ke/Kc < 0.1 | Corrosion | (2) |
| 1> Ke/Kc ≥0.1 | Corrosion -erosion | (3) |
| 10>Ke/Kc ≥1 | Erosion- Corrosion | (4) |
| Ke/Kc ≥10 | Erosion-dominated | (5) |

Where Ke is the total erosion and Kc the total corrosion contribution.
For the water environment, Fig. 9(a) the passivation-erosion environment dominates at intermediate and high impact angles at 0 mV. At potentials lower than -300 mV, in cathodic conditions, erosion-dissolution is dominant. The erosion-passivation dominated regime prevails at intermediate to low impact angles and high potentials i.e. at 400 mV and this is attributed to enhanced film formation in such conditions and the reduction in cutting intensity of eroding particles at lower impact angles. For the crude oil environment, Fig. 9(b), the total area of the map is erosion-dominated, indicating a very low contribution of corrosion in such conditions and consistent with the results, Figs. 3-7. In the oil/water conditions, Fig. 9(c) the map is dominated by erosion-passivation, at potentials greater than -300mV. Below such potentials, erosion-dissolution prevails. The fact that the more corrosion affected regime, passivation-erosion, is not observed here, unlike in the water conditions, Fig. 9(a), is due to the lower corrosion rate in the oil/water conditions compared to the water only environment, Fig 3.

Clearly such maps have important applications to oil production processes as they provide a means of identifying the conditions and environment where crude oil conditions may inhibit erosion and corrosion. The regime distinctions can highlight windows of conditions where the interactions of erosion and corrosion may be significant. Further work will be to investigate the effect of other parameters in such conditions such as particle concentration in addition to mapping the synergy/antagonism between erosion-corrosion for the parameters studied above.

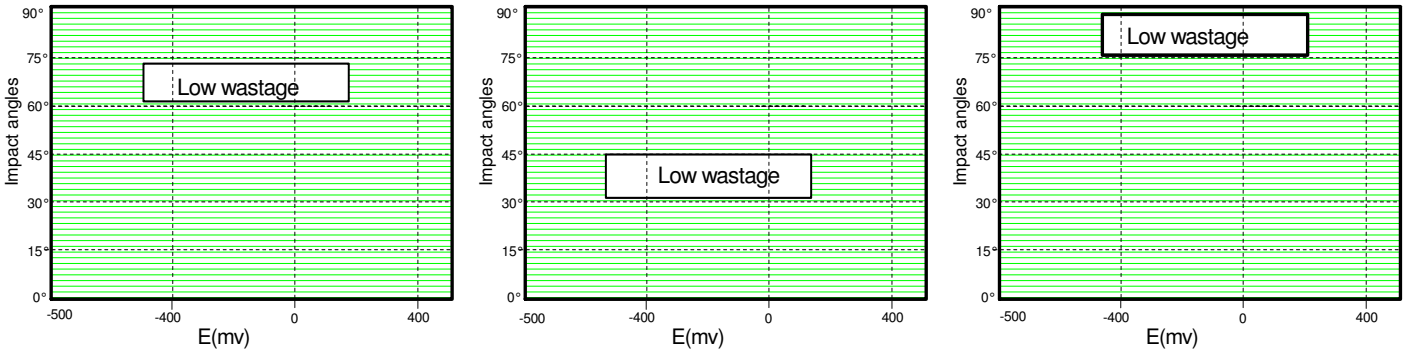


Figure (8) Erosion-corrosion wastage maps for carbon steel in (a) water, (b) crude oil and (c) crude oil / 20% of water at 2.5 m $s^{-1}$

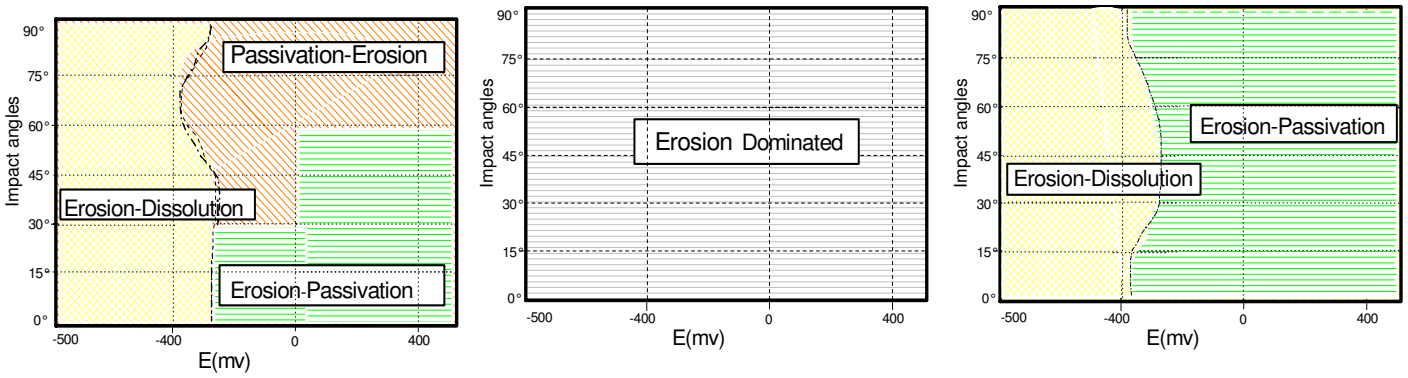


(a) (b) (c)

Figure (9) Erosion-corrosion Mechanism maps for carbon steel in (a) water, (b) crude oil and (c) crude oil / 20% of water at 2.5 m $s^{-1}$.

Table (1) Volume loss as function of impact angle for carbon steel at impact velocity 2.5 m $s^{-1}$ in water.

(a ) -400mV

| Impact angle | Ke(mg $cm^{-2}$ $h^{-1}$) | Kc(mg $cm^{-2}$ $h^{-1}$) | Kec(mg $cm^{-2}$ $h^{-1}$) |
|---|---|---|---|
| 15° | 2.59 | 1.72 | 4.31 |
| 30° | 2.5 | 1.5 | 4 |
| 45° | 2.39 | 2.21 | 4.6 |
| 60° | 2.16 | 2.04 | 4.2 |
| 75° | 1.96 | 1.93 | 3.89 |
| 90° | 2.5 | 1.71 | 4.21 |

(b) 0mV

| Impact angle | Ke(mg $cm^{-2}$ $h^{-1}$) | Kc(mg $cm^{-2}$ $h^{-1}$) | Kec(mg $cm^{-2}$ $h^{-1}$) |
|---|---|---|---|
| 15° | 2.58 | 1.82 | 4.4 |
| 30° | 2.38 | 1.83 | 4.2 |
| 45° | 1.7 | 2.71 | 4.4 |
| 60° | 1.25 | 2.25 | 3.5 |
| 75° | 2.16 | 2.46 | 4.6 |
| 90° | 1.57 | 2.73 | 4.3 |

(c) 400mV

| Impact angle | Ke(mg cm $^{-2}$ h$^{-1}$) | Kc(mg cm $^{-2}$ h$^{-1}$) | Kec(mg cm $^{-2}$ h$^{-1}$) |
|---|---|---|---|
| 15° | 2.44 | 1.97 | 4.41 |
| 30° | 2.16 | 2.07 | 4.2 |
| 45° | 3.16 | 2.16 | 5.3 |
| 60° | 2.57 | 1.93 | 4.5 |
| 75° | 0.71 | 2.74 | 3.5 |
| 90° | 1.48 | 2.53 | 4 |

Table (2) Volume loss as function of impact angle for carbon steel at impact velocity 2.5 m s$^{-1}$ in crude oil.

(a ) -400mV

| Impact angle | Ke(mg cm $^{-2}$ h$^{-1}$) | Kc(mg cm $^{-2}$ h$^{-1}$) | Kec(mg cm $^{-2}$ h$^{-1}$) |
|---|---|---|---|
| 15° | 2.479 | 2.11E-02 | 2.5 |
| 30° | 1.988 | 1.22E-02 | 2 |
| 45° | 2 | 1.02E-02 | 2.01 |
| 60° | 2.082 | 1.85E-02 | 2.1 |
| 75° | 2.1 | 2.02E-02 | 2.12 |
| 90° | 2.092 | 1.81E-02 | 2.11 |

(b ) 0mV

| Impact angle | Ke(mg cm $^{-2}$ h$^{-1}$) | Kc(mg cm $^{-2}$ h$^{-1}$) | Kec(mg cm $^{-2}$ h$^{-1}$) |
|---|---|---|---|
| 15° | 3.383 | 1.85E-02 | 3.401 |
| 30° | 3.103 | 1.71E-02 | 3.12 |
| 45° | 3.126 | 1.39E-02 | 3.14 |
| 60° | 3.381 | 1.90E-02 | 3.4 |
| 75° | 3.24 | 1.98E-02 | 3.26 |
| 90° | 3.38 | 2.00E-02 | 3.4 |

(c ) 400mV

| Impact angle | Ke(mg cm $^{-2}$ h$^{-1}$) | Kc(mg cm $^{-2}$ h$^{-1}$) | Kec(mg cm $^{-2}$ h$^{-1}$) |
|---|---|---|---|
| 15° | 4.289 | 2.14E-02 | 4.31 |
| 30° | 3.515 | 1.52E-02 | 3.53 |
| 45° | 4.185 | 1.48E-02 | 4.2 |
| 60° | 3.977 | 2.31E-02 | 4 |
| 75° | 3.686 | 2.40E-02 | 3.71 |
| 90° | 4.084 | 2.65E-02 | 4.11 |

Table (3) Volume loss as function of impact angle for carbon steel at impact velocity 2.5 m s$^{-1}$ in 20% water /crude oil.

( a) -400mV

| Impact angle | Ke(mg cm $^{-2}$ h$^{-1}$) | Kc(mg cm $^{-2}$ h$^{-1}$) | Kec(mg cm $^{-2}$ h$^{-1}$) |
|---|---|---|---|
| 15° | 2.31 | 0.8 | 3.11 |
| 30° | 1.92 | 0.78 | 2.7 |
| 45° | 2.16 | 0.84 | 3 |
| 60° | 2.42 | 0.78 | 3.2 |
| 75° | 1.96 | 1 | 2.96 |
| 90° | 2.18 | 0.9 | 3.08 |

( b ) 0mV

| Impact angle | Ke(mg cm $^{-2}$ h$^{-1}$) | Kc(mg cm $^{-2}$ h$^{-1}$) | Kec(mg cm $^{-2}$ h$^{-1}$) |
|---|---|---|---|
| 15° | 2.06 | 0.78 | 2.84 |
| 30° | 2.71 | 0.8 | 3.51 |
| 45° | 2.84 | 0.76 | 3.6 |
| 60° | 2.68 | 0.82 | 3.5 |
| 75° | 2.1 | 0.9 | 3 |
| 90° | 2.13 | 0.78 | 2.91 |

( c ) 400mV

| Impact angle | Ke(mg cm $^{-2}$ h$^{-1}$) | Kc(mg cm $^{-2}$ h$^{-1}$) | Kec(mg cm $^{-2}$ h$^{-1}$) |
|---|---|---|---|
| 15° | 1.89 | 0.71 | 2.6 |
| 30° | 2.68 | 0.72 | 3.4 |
| 45° | 2.1 | 0.9 | 3 |
| 60° | 2.02 | 0.78 | 2.8 |
| 75° | 2.23 | 0.67 | 2.9 |
| 90° | 2.4 | 0.8 | 3.2 |

**4. *Conclusions***

• The effects of impact angle and electrochemical potential on the erosion–corrosion of carbon steel X52 have been assessed in three environments containing sand particles: reservoir water, crude oil, and 20% water /crude oil.

• The results indicate that the different erosion-corrosion regimes have been identified in the various environments.

• Erosion-corrosion maps have been constructed based on the results.

**References**


1- G.A. Zhang, Y.F.Cheng (2009), Electrochemical corrosion of X65 pipe steel in oil/water emulsion, Corrosion Science, 51, pp. 901–907.

2. M.M. Stack, T.M .Abd El Badia (2006), Mapping erosion–corrosion of WC/Co–Cr based composite coatings: particle velocity and applied potential effects, Surface and Coatings Technology, 201, pp. 1335-1347.

3. R .Hamzah, D.J. Stephenson and J.E. Strutt (1995), Erosion of material used in petroleum production, Wear, 186-187, pp. 493-496.

4. A. Neville, C. Wang (2009), Erosion–corrosion of engineering steels—can it be managed by use of chemicals?, Wear, 267, pp. 2018–2026.

5- M.M. Stack, T.M .Abd El Badia (2006), On the construction of erosion–corrosion maps for WC/Co–Cr based coatings in aqueous conditions, Wear, 261, pp.1181-1190.

6. M.M. Stack, G.H. Abdulrahman (2010), Mapping erosion-corrosion of carbon steel in oil exploration conditions: Some new approaches to characterizing mechanisms and synergies, Tribology International, doi:10.1016/j.triboint.2010.01.005.

7. M.M. Stack, B.D Jana (2004), Modelling particulate erosion–corrosion in aqueous slurries: some views on the construction of erosion–corrosion maps for a range of pure metals, Wear, 256, pp. 986-1004.

8. J. B .Zu, I.M. Hutchings and G. T.Burstein (1990), Design of a slurry erosion test rig , Wear, 140, pp.331-344.

9. B.R. Tian, Y.F. Cheng (2008), Electrochemical corrosion behavior of X-65 steel in the simulated oil sand slurry. I. Effects of hydrodynamic condition, Corrosion Science , 50, pp.773-779.